INL/CON-09-15563
PREPRINT

High-Temperature Electrolysis for Large-Scale Hydrogen and Syngas Production from Nuclear Energy – System Simulation and Economics

International Conference on Hydrogen Production

J. E. O'Brien
M. G. McKellar
E. A. Harvego
C. M. Stoots

May 2009

HIGH-TEMPERATURE ELECTROLYSIS FOR LARGE-SCALE HYDROGEN AND SYNGAS PRODUCTION FROM NUCLEAR ENERGY – SYSTEM SIMULATION AND ECONOMICS

J. E. O'Brien, M. G. McKellar, E. A. Harvego, C. M. Stoots
Idaho National Laboratory
2525 N. Fremont Ave., Idaho Falls, ID USA
james.obrien@inl.gov

ABSTRACT

A research and development program is under way at the Idaho National Laboratory (INL) to assess the technological and scale-up issues associated with the implementation of solid-oxide electrolysis cell technology for efficient high-temperature hydrogen production from steam. This work is supported by the US Department of Energy, Office of Nuclear Energy, under the Nuclear Hydrogen Initiative. This paper will provide an overview of large-scale system modeling results and economic analyses that have been completed to date. System analysis results have been obtained using the commercial code UniSim, augmented with a custom high-temperature electrolyzer module. Economic analysis results were based on the DOE H2A analysis methodology. The process flow diagrams for the system simulations include an advanced nuclear reactor as a source of high-temperature process heat, a power cycle and a coupled steam electrolysis loop. Several reactor types and power cycles have been considered, over a range of reactor outlet temperatures. Pure steam electrolysis for hydrogen production as well as coelectrolysis for syngas production from steam/carbon dioxide mixtures have both been considered. In addition, the feasibility of coupling the high-temperature electrolysis process to biomass and coal-based synthetic fuels production has been considered. These simulations demonstrate that the addition of supplementary nuclear hydrogen to synthetic fuels production from any carbon source minimizes emissions of carbon dioxide during the production process.

INTRODUCTION

Currently there is increasing interest in the development of large-scale non-fossil hydrogen production technologies. This interest is driven by the immediate demand for hydrogen for refining of increasingly low-quality petroleum resources, the expected intermediate-term demand for carbon-neutral synthetic fuels, and the potential long-term demand for hydrogen as an environmentally benign direct transportation fuel [1]. At present, worldwide hydrogen production is based primarily on steam reforming of methane. From a long-term perspective, methane reforming is not a viable process for large-scale production of hydrogen since natural gas is a non-renewable resource that exhibits large volatility in price and since methane reforming and other fossil-fuel conversion processes emit large quantities of greenhouse gases to the environment. Non-fossil carbon-free options for hydrogen production include conventional water electrolysis coupled to either renewable (e.g., wind) energy sources or nuclear energy. The renewable-hydrogen option may be viable as a supplementary source, but would be very expensive as a large-scale stand-alone option [2]. Conventional electrolysis coupled to nuclear base-load power can approach economical viability when combined with off-peak power, but the capital cost is high [3]. To achieve higher overall hydrogen production efficiencies, high-temperature thermochemical [4] or electrolytic [5] processes can be used. The required high temperature process heat can be based on concentrated solar energy [6] or nuclear energy from advanced high-temperature reactors [7]. Development and demonstration of advanced nuclear hydrogen technologies are the objectives of the DOE Nuclear Hydrogen Initiative [8].

High-temperature nuclear reactors have the potential for substantially increasing the efficiency of hydrogen production from water, with no consumption of fossil fuels, no production of greenhouse gases, and no other forms of air pollution. Water-splitting for hydrogen production can be accomplished via high-temperature electrolysis (HTE) or thermochemical processes, using high-temperature nuclear process heat. In order to achieve competitive efficiencies, both processes require high-temperature operation (~850°C). Thus these hydrogen-production technologies are tied to the development of advanced high-temperature nuclear reactors. High-temperature electrolytic water-splitting supported by nuclear process heat and electricity has the potential to produce hydrogen with overall thermal-to-hydrogen efficiencies of 50% or higher, based on high heating value. This efficiency is near that of the thermochemical processes [9, 10], but without the severe corrosive conditions of the thermochemical processes and without the fossil fuel consumption and greenhouse gas emissions associated with hydrocarbon processes.

A schematic depiction of a high-temperature gas-cooled reactor coupled to a high-temperature electrolysis system is shown in Fig. 1. In this scheme, the primary helium coolant serves as the working fluid to drive a gas-turbine power cycle, which provides the electrical energy required for the high-temperature electrolysis process. In addition, some of the hot helium is used to deliver high-temperature nuclear process heat directly to the endothermic HTE process. The combination of a high-efficiency power cycle and the

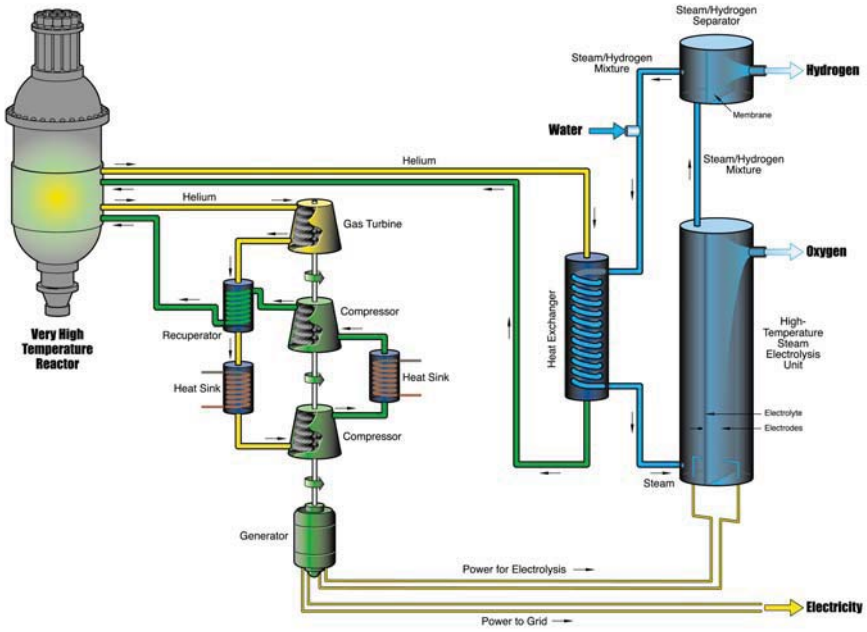

Figure 1. Schematic of high-temperature electrolysis system coupled to an advanced nuclear reactor.

direct utilization of nuclear process heat yields a high overall thermal-to-hydrogen conversion efficiency of 50% or higher.

A research program is under way at the Idaho National Laboratory (INL) to simultaneously address the technical and scale-up issues associated with the implementation of solid-oxide electrolysis cell technology for efficient hydrogen production from steam. We are coordinating a progression of electrolysis cell and stack testing activities, at increasing scales, along with a continuation of supporting research activities in the areas of materials development, single-cell testing, detailed computational fluid dynamics (CFD) analysis and system modeling.

The INL HTE program also includes an investigation of the feasibility of producing syngas by simultaneous electrolytic reduction of steam and carbon dioxide (coelectrolysis) at high temperature using solid-oxide cells. Syngas, a mixture of hydrogen and carbon monoxide, can be used for the production of synthetic liquid fuels via Fischer-Tropsch processes. This concept, coupled with nuclear energy, provides a possible path to reduced greenhouse gas emissions and increased energy independence, without the major infrastructure shift that would be required for a purely hydrogen-based transportation system [11 - 14]. Furthermore, if the carbon dioxide feedstock is obtained from biomass, the entire concept would be climate-neutral.

HTE PLANT PROCESS MODELS

A number of detailed process models have been developed for large-scale system analysis of high-temperature electrolysis plants. These analyses have been performed using UniSim process analysis software [15]. UniSim is a derivative of HYSYS. The software inherently ensures mass and energy balances across all components and includes thermodynamic data for all chemical species. The overall process flow diagram for a very high-temperature helium-cooled reactor (VHTR) coupled to the direct helium recuperated Brayton power cycle and the HTE plant with air sweep is presented in Fig. 2 [10]. The reactor thermal power assumed for the high-temperature helium-cooled reactor is 600 MW_{th}. The primary helium coolant exits the reactor at 900°C. This helium flow is split at T1, with more than 90% of the flow directed toward the power cycle and the remainder directed to the intermediate heat exchanger to provide process heat to the HTE loop. Within the power-cycle loop, helium flows through the power turbine where the gas is expanded to produce electric power. The helium, at a reduced pressure and temperature, then passes through a recuperator and precooler where it is further cooled before entering the low-pressure compressor. To improve compression efficiencies, the helium is again cooled in an intercooler heat exchanger before entering the high-pressure compressor. The helium exits the high-pressure compressor at a pressure that is slightly higher than the reactor operating pressure of 7 MPa. The coolant then circulates back through the recuperator where the recovered heat raises its temperature to the reactor inlet temperature of 647°C, completing the cycle.

Liquid water feedstock to the HTE process enters at the left in the diagram. The water is compressed to the HTE process pressure of 3.5 MPa in the liquid phase using a pump. The HTE process is operated at elevated pressure for two reasons. Elevated pressure supports higher mass flow rates for the same size

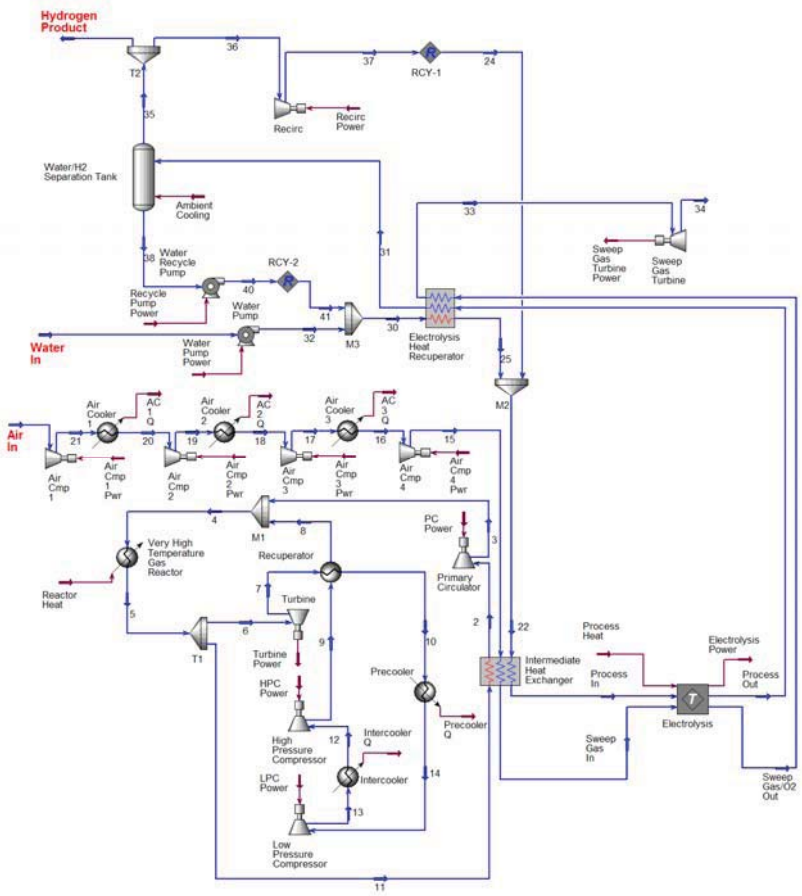

Figure 2. Process flow diagram for a helium-cooled reactor/direct Brayton/HTE system with air sweep.

components. Furthermore, the gaseous hydrogen product will ultimately be delivered at elevated pressure either for storage or pipeline. Therefore, from the standpoint of overall process efficiency, it is logical to compress the liquid water feedstock at the process inlet since liquid-phase compression work is very small compared to compression of the gaseous product.

Downstream of the pump, condensate from the water knockout tank is recycled back into the inlet stream at M3. The water stream is then vaporized and pre-heated in the electrolysis recuperator, which recovers heat from the post-electrolyzer process and sweep-gas outlet streams. Downstream of the recuperator, at M2, the steam is mixed with recycled hydrogen product gas. A fraction of the product gas is recycled in this way in order to assure that reducing conditions are maintained on the steam/hydrogen electrode. Downstream of the mixer, the process gas mixture enters the intermediate heat exchanger (IHX), where final heating to the electrolysis operating temperature occurs, using high-temperature process heat from the nuclear reactor. The process stream then enters the electrolyzer, where the steam is electrolytically reduced, yielding hydrogen on the cathode side of each cell and oxygen on the anode side. Most of the components included in the process flow diagram are standard UniSim components. However, a custom electrolyzer module was developed at INL for direct incorporation into the UniSim system analysis code, as described in detail in reference [16].

Downstream of the electrolyzer, the hydrogen-rich product stream flows through the electrolysis recuperator where it is cooled and the inlet process stream is preheated. The cooled product stream is split at T2 and a fraction of the product gas is recycled into the inlet process stream, as discussed previously. A recirculating blower is required to repressurize the recycle stream to the upstream pressure at M2. The remainder of the product stream is cooled further at the water knockout tank, where the majority of any residual steam is condensed and separated, yielding dry hydrogen product.

The process flow diagram shows air in use as a sweep gas, to remove the excess oxygen that is evolved on the anode side of the electrolyzer. For the air-sweep cases, inlet air is compressed to the system operating pressure of 3.5 MPa in a four-stage compressor with intercooling. The final compression stage is not followed by a cooler, so the air enters the IHX at about 120°C. The sweep gas is heated to the electrolyzer operating temperature of 800°C via the IHX which supplies high-temperature nuclear process heat directly to the system. The sweep gas then enters the electrolyzer, where it is combined with product oxygen. Finally, it passes through the electrolysis recuperator to help preheat the incoming process gas.

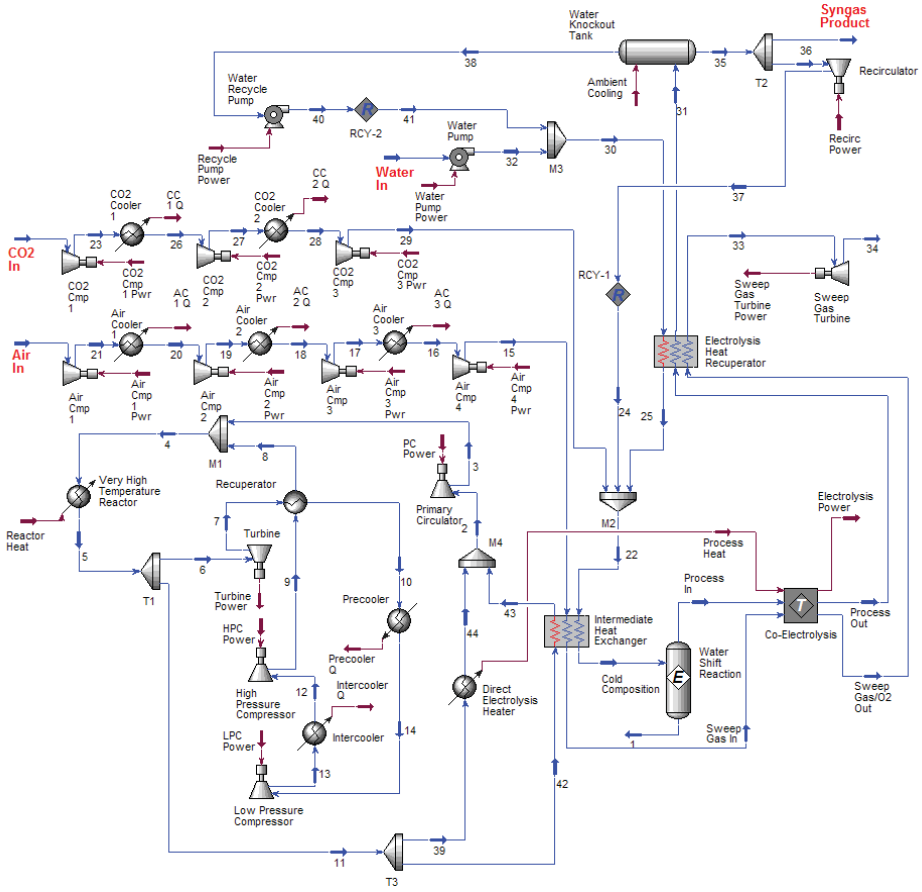

Figure 3. Process flow diagram for co-electrolysis plant.

Some of the sweep gas compression work is recovered using a sweep-gas turbine located at the sweep-gas exit.

In order to avoid the work requirement associated with compression of the sweep gas, it is possible to operate with no sweep gas, and to allow the system to produce pure oxygen, which could potentially be supplied to another collocated process such as an oxygen-blown gasifier. For this mode of operation, the four-stage air compressor would not be included in the process flow diagram and there would be no air flow through the intermediate heat exchanger. Air preheat at the IHX is no longer needed. Oxygen would simply be evolved from the anode side of the electrolyzer at the electrolysis operating pressure and temperature. It would flow through the electrolysis heat recuperator and the outlet turbine. The results of our system analyses have shown that this concept is desirable from the standpoint of overall process efficiency, but there are significant technical issues associated with handling high-temperature pure oxygen that would have to be addressed.

Similar system analyses have been performed to evaluate the concept of direct syngas production from steam and carbon dioxide using HTE. A graphical representation of the process model developed for this study is presented in Fig. 3. The primary process feedstock streams are liquid water and carbon dioxide. The inlet water stream is compressed in the liquid phase to the process operating pressure of 3.5 MPa using a pump. This operating pressure was selected because it is approximately equal to the desired operating pressure for a Fisher-Tropsch process using a cobalt catalyst. Downstream of the pump, condensate from the water knockout tank is recycled back into the inlet stream at M3. The water stream is then vaporized and pre-heated in the electrolysis recuperator, which recovers heat from the post-electrolyzer process and sweep-gas outlet streams. Downstream of the recuperator, at M2, the steam is mixed with carbon dioxide plus recycled hydrogen and carbon monoxide product gas. A fraction of the product gas is recycled in this way in order to ensure that reducing conditions are maintained on the steam/hydrogen electrode. Downstream of the mixer, the process gas mixture enters the intermediate heat exchanger (IHX), where final heating to the electrolysis operating temperature occurs, using high-temperature process heat from the nuclear reactor. A gas shift reaction occurs with the heated gas mixture represented by an equilibrium reactor in the process flow diagram, allowing chemical equilibrium to be achieved. The process stream then enters the electrolyzer, where oxygen is electrolytically removed from the system, producing hydrogen and carbon monoxide.

For these simulations, the per-cell active area for electrolysis was assumed to be 225 cm^2. This cell size is well within the limits of current technology for planar cells. Area-specific resistance (*ASR*) was used to characterize the performance of the electrolysis cells. This parameter incorporates the loss mechanisms in the cells. The *ASR* value used in the electrolyzer module is temperature-dependent per the following Arrhenius equation:

$$ASR(T) = ASR_{1100K} - 0.463 + 3.973 \times 10^{-5} \exp\left(\frac{10300}{T(K)}\right) \quad (1)$$

where ASR_{1100K} represents the user-specified cell ASR at the temperature 1100 K (e.g., 0.25 or 1.25). This constant allows one to shift the entire *ASR* curve to higher or lower *ASR* values, to mimic lower or higher performing cells, respectively. This equation for *ASR(T)* is based on empirical data obtained from an actual operating stack, modified to allow user specification of the *ASR* value at 1100 K. In order to show the trends that can be expected with higher or lower ASR, two values of ASR_{1100K} have been included in this study. The ASR_{1100K} value of 1.25 represents a stack-average *ASR* value at 1100 K that is achievable in the short term with existing technology. The ASR_{1100K} value of 0.25 is an optimistic value that has been observed in button cells, but will be difficult to achieve in a stack in the short term. The temperature dependence of the *ASR* is important for the adiabatic cases (since the outlet temperature in these cases is generally different than the inlet temperature) and for evaluating the effect of electrolyzer inlet temperature on overall process efficiency.

The total number of cells used in the process simulations was determined by specifying a maximum current density for each *ASR* value considered that was large enough to ensure that the operating voltage would just exceed the thermal neutral voltage. For the higher nominal *ASR* value of 1.25 Ohm·cm^2, the maximum current density was set at 0.25 A/cm^2 and an adiabatic thermal boundary condition was assumed. The total number of cells for this base case was adjusted until the total remaining power was zero. In other words, the full power cycle output at this operating point is dedicated to electrolysis. This procedure resulted in 1.615×10^6 cells required. At lower current densities, the power cycle output exceeds the value required for electrolysis and this excess power would be supplied to the grid. For the case of *ASR* = 0.25 Ohm·cm^2, the maximum current density was set at 1.0 A/cm^2. A much higher maximum current density was required for the lower *ASR* case, again in order to assure that the thermal neutral voltage was just exceeded.

Two thermal boundary condition limits were considered for the electrolyzer: isothermal and adiabatic. Actual electrolyzer operation will generally lie between these limits. For the isothermal cases, heat from the reactor was directly supplied to the electrolyzer to maintain isothermal conditions for operation below the thermal neutral voltage. Heat rejection from the electrolzer is required to maintain isothermal operation at operating voltages above thermal neutral. For the adiabatic cases, the direct electrolyzer heater shown in Fig. 3 was not used.

To allow for comparisons between the performance of the HTE processes to alternate hydrogen and syngas production techniques, we have adopted a general efficiency definition that can be applied to any thermal water-splitting, or syngas production process, including HTE, low-temperature electrolysis (LTE), thermochemical water splitting, co-electrolysis, coal-to-syngas, and biomass-to-syngas. Since the primary energy input to the thermochemical processes is in the form of heat, the appropriate general efficiency definition to be applied to all of the techniques is the overall thermal-to-hydrogen efficiency, η_H. This efficiency is defined as the heating value of the product hydrogen (plus CO for syngas production processes) divided by the total thermal input required to produce it. In this report, the lower heating value, LHV, of the products has been used:

$$\eta_H = \frac{\sum_i \dot{N}_i LHV_{i,product}}{\sum_i \dot{Q}_i + \sum_i \dot{N}_i LHV_{i,reactant}} \quad (2)$$

The denominator in this efficiency definition quantifies all of the net thermal energy that is consumed in the process plus the heating value of any feedstock reactants, such as coal or biomass. For a thermochemical process, this summation includes the direct nuclear process heat as well as the thermal equivalent of any electrically driven components such as pumps, compressors, etc. The thermal equivalent of any electrical power consumed in the process is the power divided by the thermal efficiency of the power cycle. The power-cycle thermal efficiency for the helium-cooled direct Brayton cycle concept described in this paper was 52.6%. For an electrolysis process, the summation in the denominator of Eqn. (1) includes the thermal equivalent of the primary electrical energy input to the electrolyzer and the secondary contributions from smaller components such as pumps and compressors. In additional, any direct thermal inputs are also included. Direct thermal inputs include any net (not recuperated) heat required to heat the process streams up to the electrolyzer operating temperature and any direct heating of the electrolyzer itself required for

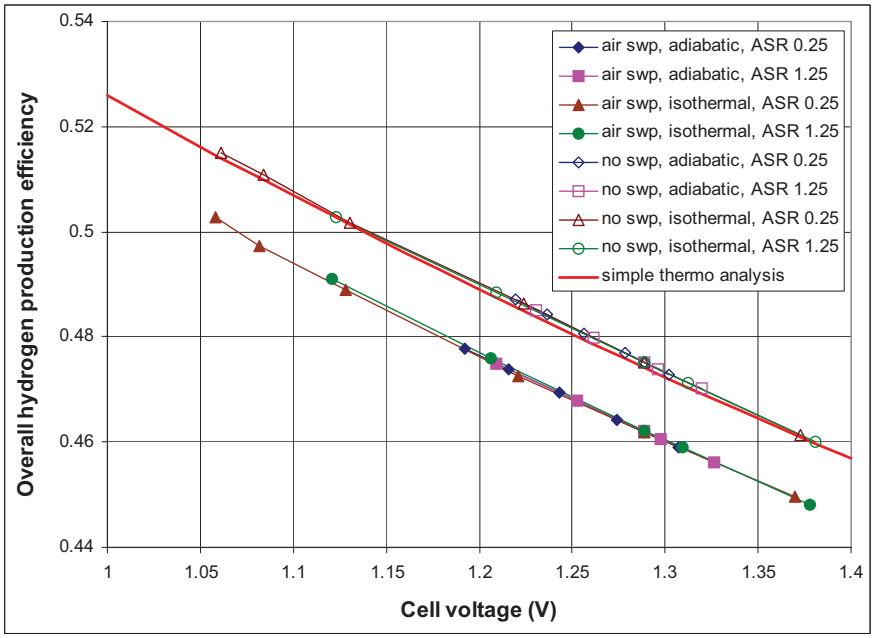

Figure 4. Overall HTE hydrogen production efficiencies for the VHTR/recuperated direct Brayton cycle, as a function of per-cell operating voltage.

isothermal operation. Note that for co-electrolysis of steam and carbon dioxide, the numerator in Eqn. (2) includes the low heating value of the produced carbon monoxide.

RESULTS

Hydrogen Production

A summary of results obtained from the hydrogen production system analyses is presented in Figs. 4 and 5. The results presented in these figures were obtained for a fixed steam utilization of 89% (i.e., 89% of the inlet steam was converted to hydrogen). In order to maintain fixed steam utilization, the flow rates of the process streams were adjusted with lower flow rates for lower current densities and higher flow rates for higher current densities. Results of eight cases are presented in Fig. 4: low and high *ASR*, adiabatic and isothermal electrolyzer operation, air-sweep and no-sweep. The figure provides overall hydrogen production efficiencies (Eqn. 2) as a function of per-cell operating voltage. Recall that electrolyzer efficiency is inversely proportional to operating voltage [17]. Higher operating voltages yield higher current densities and higher hydrogen production rates, but lower overall efficiencies, so the selection of electrolyzer operating condition is a tradeoff between production rate and efficiency. For a specified target production rate, higher production efficiency requires a higher capital cost, since more cells would be required to achieve the target production rate. In general, a good tradeoff between production rate and efficiency occurs for operating voltages near or slightly below the thermal neutral value, around 1.29 V. This operating voltage is also desirable from the standpoint that the electrolysis stack operates nearly isothermally at this voltage. Predicted overall thermal-to-hydrogen efficiency values shown in Fig. 4 are generally within 8 percentage points of the power-cycle efficiency of 52.6%, decreasing with operating voltage. It is interesting to note that the overall process efficiencies for these fixed-utilization cases collapse onto individual lines, one for the air-sweep cases and another for the no-sweep cases, when plotted as a function of per-cell operating voltage, regardless of the electrolyzer mode of operation (adiabatic or isothermal) and ASR value. Note that the highest operating voltages shown are just above the thermal neutral voltage of 1.29 V. Note also that the highest overall efficiency plotted in Fig. 4 (for no-sweep, *ASR* = 0.25, isothermal, V = 1.06 A/cm^2) exceeds 51%.

An additional line, based on a simple thermodynamic analysis [17] is also shown in Fig. 4. This analysis considers a control volume drawn around the electrolysis process, with the process consuming the electrical work from the power cycle, and heat from a high-temperature source. If the inlet and outlet streams are assumed to be liquid water, and gaseous hydrogen and oxygen, respectively, at $T = T^o$, $P = P^o$, direct application of the first law, Faraday's law, and the definition of the overall thermal-to-hydrogen efficiency yields:

$$\eta_H = \frac{LHV}{2FV_{op}(1/\eta_{th} - 1) + HHV} \tag{3}$$

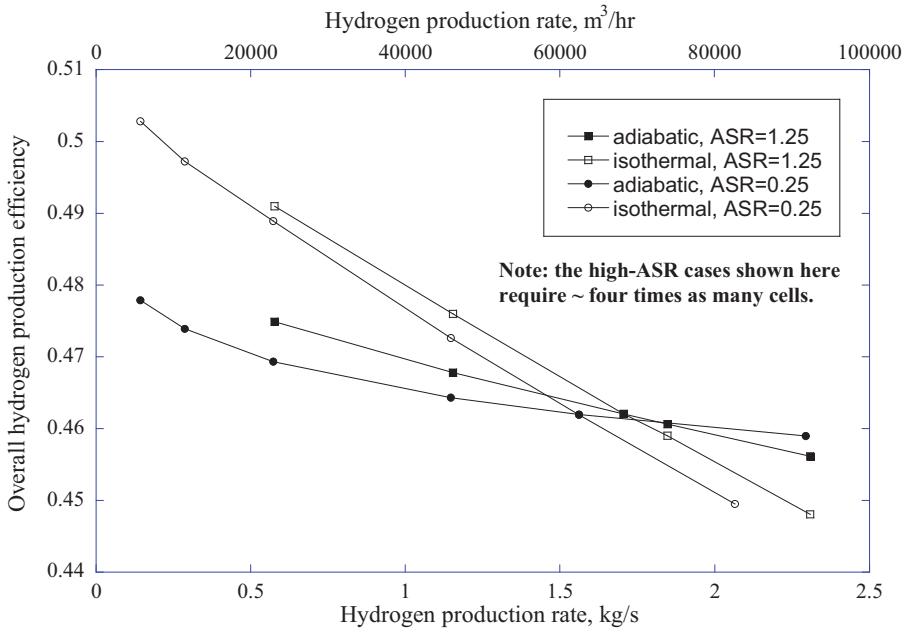

Figure 5. Overall hydrogen production efficiency as a function of hydrogen production rate, with air sweep.

The curve labeled "simple thermo analysis" in Fig. 4 represents Eqn. (3). This equation provides a useful reference against which detailed system analyses can be measured. The simple thermodynamic analysis agrees quite closely with the detailed system analysis results for the no-sweep cases, which correspond directly with the conditions of simple analysis since it does not include consideration of a sweep gas. Overall hydrogen efficiency results of the air-sweep cases are about 1% lower than the no-sweep cases.

Hydrogen production efficiencies can also be plotted as a function of hydrogen production rate, as shown in Fig. 5. As expected, efficiencies decrease with production rate since higher production rates require higher current densities and higher per-cell operating voltages, for a fixed number of cells. For this plot, the full 600 MW_{th} output of the reactor is assumed to be dedicated to hydrogen production. Under this assumption about four times as many electrolysis cells are required for the high-ASR cases than for the low-ASR cases, with a correspondingly higher associated capital cost. Fig. 5 shows that hydrogen production rates in excess of 2.3 kg/s (92,000 SCMH, 78×10^6 SCF/day) could be achieved with a dedicated 600 MW_{th} hydrogen-production plant. This rate is the same order of magnitude as a large hydrogen production plant based on steam-methane reforming. Fig. 5 indicates similar overall efficiencies for the low-*ASR* and high-*ASR* cases at a specified electrolyzer thermal operating condition (adiabatic or isothermal) and hydrogen production rate.

The effect of steam utilization was examined by fixing the electrolyzer inlet process gas flow rates at the values corresponding to the highest current density achievable with each ASR value, then varying the current density over the full range of values considered for the fixed-utilization cases. Low current densities for this case yield low values of steam utilization since the inlet steam flow rate is fixed at a value that yields 89% utilization at the highest current density. Results of this exercise are presented in Fig. 6. The overall efficiency results for the variable-utilization cases nearly collapse onto a single curve when plotted versus utilization. The plot indicates a strong dependence on utilization, with overall hydrogen production efficiencies less than 25% at the lowest utilization values shown (~5.5%), increasing to a maximum value of ~47% at the highest utilization value considered (89%). So, from the overall system perspective, low steam utilization is bad. This is an interesting result because, from the perspective of the electrolyzer alone, low utilization yields high electrolyzer (not overall) efficiency values. Excess steam in the electrolyzer keeps the average Nernst potential low for each cell, which assures a low operating voltage for a specified current density (or hydrogen production rate). However, from the overall system perspective, low steam utilization means that the system is processing lots of excess material, resulting in relatively high irreversibilities associated with incomplete heat recuperation, pumping and compression of excess process streams, etc. Above ~50% utilization, however, the efficiency curves are relatively flat, even decreasing slightly for the isothermal cases. Regarding very high utilization values, achievement of steam utilization values much above 90% is not practical from an operational standpoint because localized steam starvation can occur on the cells, with associated severe performance penalties and possible accelerated cell lifetime degradation.

The effect of reactor outlet temperature has also been considered. Fig. 7 shows overall hydrogen production efficiencies, based on high heating value in this case, plotted as a function of reactor outlet

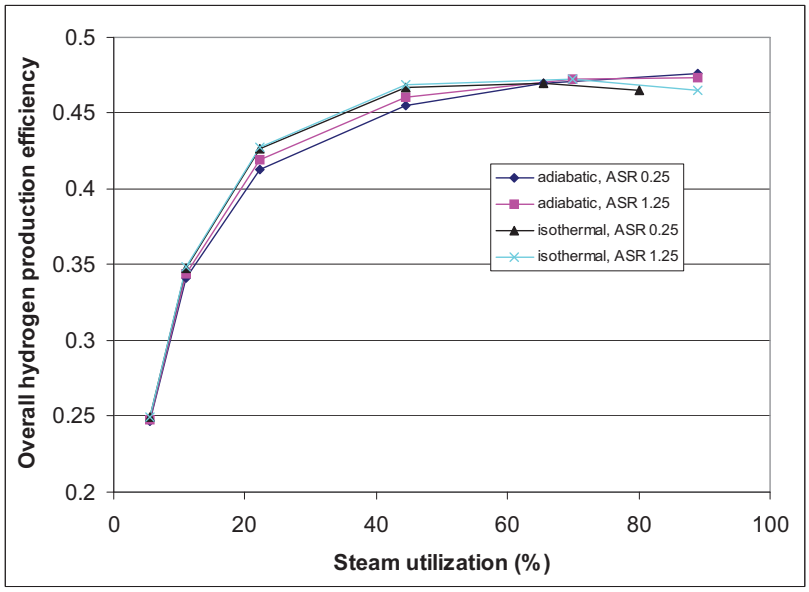

Figure 6. Effect of steam utilization on overall hydrogen production efficiency.

temperature. The figure includes a curve that represents 65% of the thermodynamic maximum possible efficiency for any thermal water splitting process, assuming heat addition occurs at the reactor outlet temperature and heat rejection occurs at T_L = 20°C [17]. In order to cover a broad range of possible reactor outlet temperatures, three different advanced-reactor/power-conversion combinations were considered: a helium-cooled reactor coupled to a direct recuperative Brayton cycle, a supercritical CO_2-cooled reactor coupled to a direct recompression cycle, and a sodium-cooled fast reactor coupled to a Rankine cycle. Each reactor/power-conversion combination was analyzed over an appropriate reactor outlet temperature range.

The figure shows results for both HTE and low-temperature electrolysis (LTE). In addition, an efficiency curve for the SI thermochemical process is shown [18]. The results presented in Fig. 7 indicate that, even when detailed process models are considered, with realistic component efficiencies, heat exchanger performance, and operating conditions, overall hydrogen production efficiencies in excess of 50% can be achieved for HTE with reactor outlet temperatures above 850°C. For reactor outlet temperatures in the range of 600 - 800°C, the supercritical CO_2/recompression power cycle is superior to the He-cooled/Brayton cycle concept. This conclusion is consistent with results presented in [9]. The efficiency curve for the SI process also includes values above 50% for reactor outlet temperatures above 900°C, but it drops off quickly

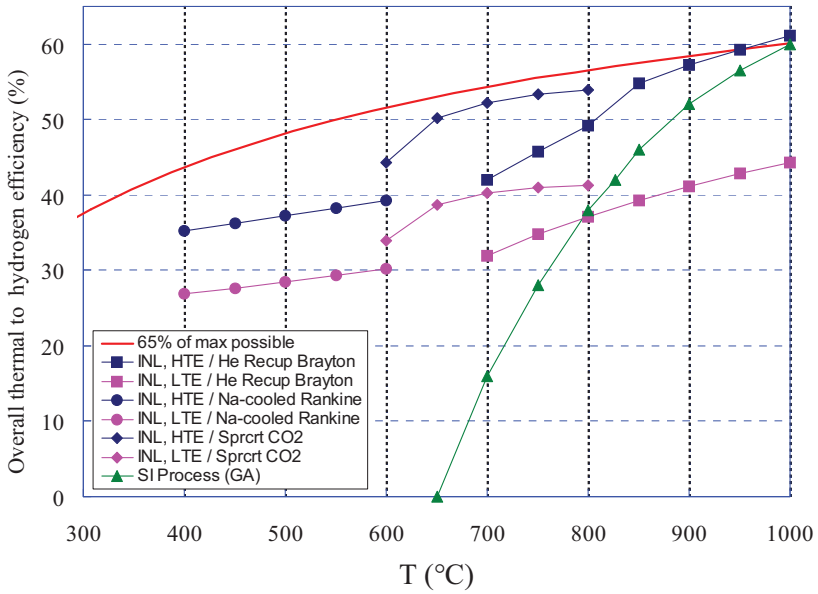

Figure 7. Overall thermal-to-hydrogen efficiencies (based on HHV) for HTE coupled to three different reactor types, as a function of reactor outlet temperature.

with decreasing temperature, and falls below values for LTE coupled to high-temperature reactors for outlet temperatures below 800°C. Note that even LTE benefits from higher reactor outlet temperatures because of the improved power conversion thermal efficiencies. Current planning for NGNP [7] indicates that reactor outlet temperatures will be at or below 850°C, which favors HTE.

Direct Electrolytic Syngas Production

System analysis results for direct syngas production from co-electrolysis of steam and CO_2 are qualitatively similar to the straight steam electrolysis results. Representative results are presented in Fig. 8. Once again, overall process efficiencies for fixed utilization collapse onto a single line when plotted as a function of per-cell operating voltage, as shown in Fig. 8(a). Note that the highest operating voltages shown are just above the co-electrolysis thermal neutral voltage of 1.34 V. Note also that the highest overall efficiency plotted in Fig. 8(a) (for ASR = 0.25, isothermal, i = 0.0625 A/cm^2) is actually slightly higher than the power cycle efficiency of 48.3%. Overall syngas production efficiencies are plotted as a function of syngas production rate in Fig. 8(b). This figure shows that syngas production rates in excess of 10 kg/s (78,000 SCMH) could be achieved with a dedicated 600 MW_{th} syngas-production plant. Fig. 8(b) also indicates similar overall efficiencies for the low-*ASR* and high-*ASR* cases at a specified electrolyzer thermal operating condition (adiabatic or isothermal) and syngas production rate. Recall, however, that the high-*ASR* plant requires four times as many cells as the low-*ASR* plant for the same syngas production rate and operating voltage. So the capital cost of the electrolytic plant would be significantly greater with the high-*ASR* cells compared to the low-*ASR* cells. Syngas production efficiencies are plotted as a function of steam/CO_2 utilization in Fig. 8(c). The overall efficiency results for the variable-utilization case nearly collapse onto a single curve when plotted versus utilization. The plot indicates a strong dependence on utilization, with overall efficiencies of only 20% at the lowest utilization values shown (~5.7%), increasing to a maximum value of 43% at the highest utilization value considered (90%). Again, low utilization results in relatively high irreversibilities associated with incomplete heat recuperation, pumping and compression of excess process streams, etc.

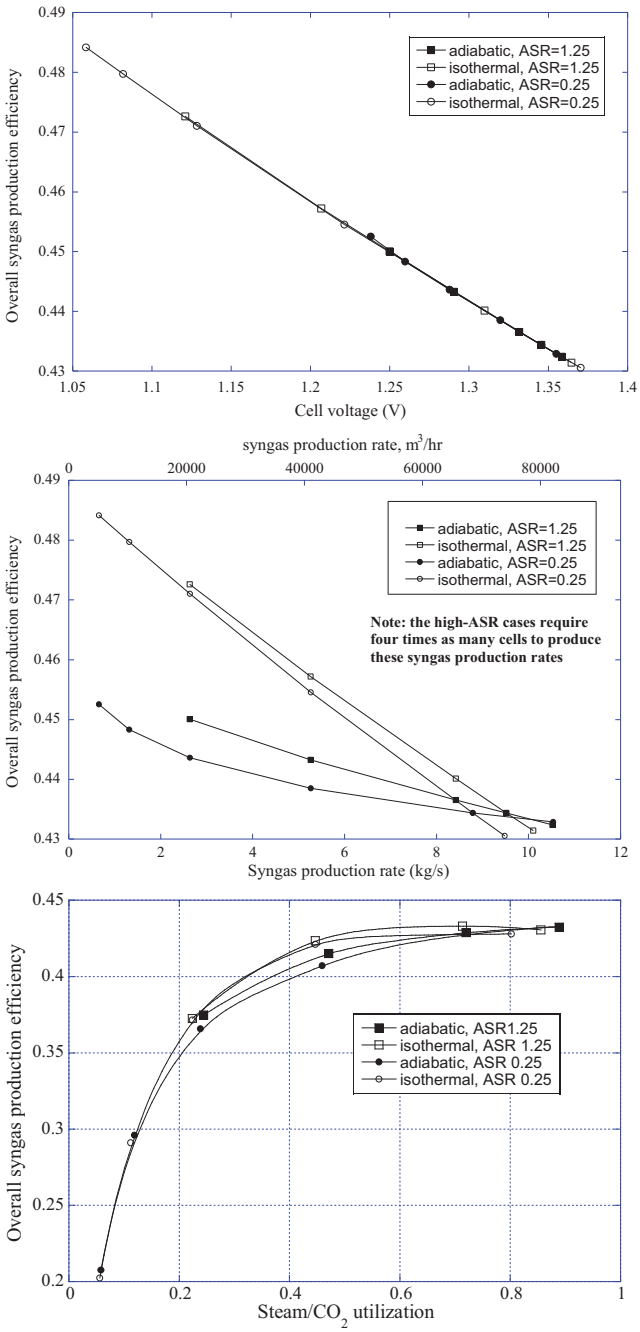

Figure 8. Overall syngas production efficiencies, air-sweep cases; (a) fixed utilization, function of per-cell operating voltage; (b) fixed utilization, function of syngas production rate; (c) variable utilization, function of utilization.

Syngas Production from Coal and Biomass

One possible strategy for reducing dependence on imported oil is to utilize alternate carbon sources like coal or biomass for the production of synthetic liquid fuels such as diesel. The first step in the production of synthetic liquid fuels is syngas production. However, the traditional processes for producing syngas from these carbon sources also produce significant quantities of carbon dioxide that must be sequestered or

released to the atmosphere. For example, with traditional coal-to-liquids (CTL) technology, only about one-third of the carbon in the coal feedstock ends up in the liquid fuel product [19]. If supplemental hydrogen is available, nearly all of the carbon in the coal can end up in the liquid fuel product. Supplemental hydrogen for this process should be obtained from an efficient non-carbon-emitting process such as high-temperature electrolysis (HTE) of steam powered by nuclear energy [5]. Coupling of the HTE process to CTL is particularly appealing because it is more efficient than conventional electrolysis and because it provides both hydrogen and oxygen at elevated temperature. The oxygen can be fed directly to a gasifier and the hydrogen can be used to reduce the excess carbon dioxide produced in the gasifier, via the reverse shift reaction. A system analysis of the nuclear/HTE-assisted CTL process has been recently completed at INL [20]. A representative result from this study is shown in Fig. 9 which shows the dependence of syngas production efficiency and carbon utilization on coal moisture content. Carbon utilization increases with decreased moisture content, reaching a value of 98.8% for a moisture content of 16.1%. The syngas production efficiency shown in Fig. 9 also appears to increase as the moisture content is reduced, but peaks at about 68.8% at a coal moisture content of 25%. The slight drop in syngas production efficiency as the coal moisture content is reduced below 25% is the result of the need to increase the gasifier temperature to maintain a minimum heat exchanger approach temperature for the steam generator of approximately 20°C. This drop in syngas production efficiency is consistent with results that show a drop in syngas production efficiency as the gasifier temperature increased. Note that the syngas production efficiencies for this process are considerably higher than those associated with the purely electrolytic co-electrolysis process. A similar study has been performed for nuclear-assisted biomass-to-syngas [21]. This study predicted biomass-to syngas efficiencies greater than 70%, with carbon utilization near 95%.

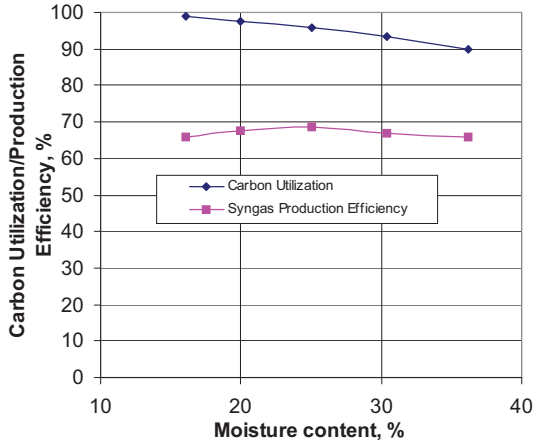

Figure 9. Carbon utilization and syngas production efficiency as a function of coal moisture content.

ECONOMIC ANALYSIS - HYDROGEN PRODUCTION

A preliminary economic analysis has also been performed to estimate the cost of hydrogen based on high-temperature electrolysis coupled to an advanced high-temperature gas-cooled reactor [22]. The reference HTE plant is driven by a 600 MW_t high-temperature helium-cooled reactor coupled to a direct Brayton power cycle with a reactor outlet temperature of 900°C. Plant parameters used in the reference plant optimization were based on parametric studies performed using the UniSim process analysis software. The economic analysis was performed using the standardized H2A Analysis Methodology developed by the Department of Energy (DOE) Hydrogen Program, using realistic financial and cost estimating assumptions. Based on this methodology, and the various assumptions discussed in detail in reference [22], the estimated price of the hydrogen leaving the plant gate at 5 MPa pressure would be $3.23/kg. This estimated price was shown to be most sensitive to the assumed after-tax internal rate of return and the cost of unplanned replacement costs. Compared to the current hydrogen commodity price of about $2.50/kg (based on steam-methane reforming), this estimated cost is not unreasonable considering the volatility of the cost of the natural gas and the fact that the HTE technology does not emit greenhouse gases. Estimates of hydrogen production cost based on LTE depend strongly on electricity prices, but for large systems (1000 kg/day), with an assumed industrial electricity cost of $0.0483/kWh, a hydrogen selling price of $4.15 (FY2000 dollars) has been reported [23], based on the DOE H2A methodology. The lesson here is that any proposed new technology for large-scale hydrogen production must be able to compete with this price.

For the economic analysis of HTE-produced hydrogen, isothermal operation of the electrolyzer was assumed. An air sweep system is also included in the reference design to remove oxygen from the anode side of the electrolyzer because of concerns with handling of the high-temperature oxygen product gas. Predicted overall thermal-to-hydrogen efficiency values for the reference design with an air-sweep system resulted in hydrogen production efficiencies that were only 1.0–1.5% lower than that for the equivalent design with no sweep-gas system [10]. The operating pressure of 5.0 MPa for the HTE process loop was selected to be consistent with the need to deliver the hydrogen product gas at elevated pressures for storage or pipeline transport. This pressure also represents a trade off between the need for larger components at lower pressures and the need for more massive components for pressure containment at higher pressures. The overall thermal-to-hydrogen efficiency for the reference case is 47.1%.

As noted above, the lifecycle cost analysis of the reference HTE design resulted in a calculated hydrogen cost of $3.23/kg, assuming an after-tax internal rate of return of 10%. This represents the cost of hydrogen leaving the plant gate, and does not include any additional storage, delivery, fuel taxes or other

costs that the consumer might pay at the pump. A breakdown of the component costs contributing to the total cost of $3.23/kg shows that capital costs account for over 70% of total costs (i.e., $2.36/kg of H_2). This is expected because of the high construction costs for the nuclear reactor. Fixed operating and maintenance costs ($0.57/kg of H_2) are relatively high because they include operation and maintenance costs for both the reactor and hydrogen production plant. Yearly variable costs ($0.28/kg of H_2) include the reactor fuel cost, a reserve for unplanned equipment replacement costs, and the yearly replacement cost of the solid oxide electrolysis cells. The cost of the SOEC modules was estimated to be $200/kW of power to the electrolysis stack and it is assumed that 1/3 of the modules are replaced annually. The feedstock cost contribution ($0.012/kg of H_2) represents the cost of the demineralized water feedstock, which feeds the electrolysis process. Although the electrolysis process also produces oxygen, which could be sold as a byproduct of the hydrogen production process, the reference HTE design does not attempt to recover the oxygen byproduct. Therefore, while the sale of the oxygen byproduct would lower the overall cost of the hydrogen production process, no credit for the production of oxygen was taken in this cost analysis.

SUMMARY AND CONCLUSIONS

Several detailed process models have been developed to evaluate large-scale system performance of high-temperature electrolysis plants coupled to advanced nuclear reactors. Results of the system analyses for high-temperature steam electrolysis predicted overall thermal-to-hydrogen efficiency values that are generally within 8 percentage points of the power-cycle efficiency of 52.6%, decreasing with per-cell operating voltage. Overall hydrogen efficiency results of the air-sweep cases are about 1% lower than the no-sweep cases. Overall efficiencies exhibit strong dependence on utilization, with overall hydrogen production efficiencies of only 20% at the lowest utilization values shown (~5.5%), increasing to a maximum value of ~48% at the highest utilization value considered (89%). Hydrogen production rates in excess of 2.3 kg/s (92,000 SCMH, 78×10^6 SCF/day) could be achieved with a dedicated 600 MW_{th} hydrogen-production plant. This rate is the same order of magnitude as a large hydrogen production plant based on steam-methane reforming. The effect of reactor outlet temperature was also considered. Results indicate that, even when detailed process models are considered, with realistic component efficiencies, heat exchanger performance, and operating conditions, overall hydrogen production efficiencies in excess of 50% can be achieved for HTE with reactor outlet temperatures above 850°C. System analysis results for direct syngas production from co-electrolysis of steam and CO_2 are qualitatively similar to the straight steam electrolysis results. Syngas production rates in excess of 10 kg/s (78,000 SCMH) could be achieved with a dedicated 600 MW_{th} syngas-production plant. We have also examined nuclear-assisted coal-to-liquids for the production of syngas, ultimately leading to synthetic liquid fuels. With supplemental nuclear hydrogen, carbon utilization from the coal can be as high as 98.8% for a coal moisture content of 16.1%, with overall syngas production efficiencies as high as 68.8%. Finally, an economic analysis was performed using the standardized H2A Analysis Methodology developed by the Department of Energy (DOE) Hydrogen Program, using realistic financial and cost estimating assumptions to estimate the cost of hydrogen based on high-temperature electrolysis coupled to an advanced high-temperature gas-cooled reactor. The estimated price of the hydrogen leaving the plant gate at 5 MPa pressure would be $3.23/kg. This estimated price was shown to be most sensitive to the assumed after-tax internal rate of return and the cost of unplanned replacement costs.

ACKNOWLEDGEMENTS

This work was supported by the U.S. Department of Energy, Office of Nuclear Energy, Nuclear Hydrogen Initiative and Next Generation Nuclear Plant Programs under DOE Operations Office Contract DE-AC07-05ID14517.

REFERENCES

1. Forsberg, C. W., “The Hydrogen Economy is Coming. The Question is Where?” *Chemical Eng. Progress*, Dec. 2005, pp. 20-22.
2. Granovskii, M., Dincer, I., and Rosen, M. A., “Greenhouse gas emissions reduction by use of wind and solar energies for hydrogen and electricity production: economic factors,” *Int. J. Hydrogen Energy*, V. 32, 2007, pp. 927-931.
3. Floch, P-H., Gabriel, S., Mansilla, C., and Werkoff, F., “On the production of hydrogen via alkaline electrolysis during off-peak periods,” *Int. J. Hydrogen Energy*, Vol. 32, 2007, pp. 4641-4647.
4. Schultz, K. R., Brown, L. C., Besenbruch, G. E. and Hamilton, C. J., “Large-Scale Production of Hydrogen by Nuclear Energy for the Hydrogen Economy,” Report GA-A24265, Feb. 2003, 22p.
5. O’Brien, J. E., Stoots, C. M., Herring, J. S., and Hartvigsen, J. J., “Performance of Planar High-Temperature Electrolysis Stacks for Hydrogen Production from Nuclear Energy,” *Nuclear Technology*, Vol. 158, pp. 118 - 131, May, 2007.
6. Steinfeld, A. “Solar thermochemical production of hydrogen,” *Solar Energy*, V 78, No 5, pp. 603-615, May 2005.

7. Southworth, F., Macdonald, P. E., Harrell, D. J., Park, C. V., Shaber, E. L., Holbrook, M. R., and Petti, D. A., "The Next Generation Nuclear Plant (NGNP) Project," Proceedings, Global 2003, pp. 276-287, 2003.
8. Schultz, K., Sink, Pickard, P., Herring, J. S., O'Brien, J. E., Buckingham, R., Summers, W., and Michele Lewis, M., "Status of the US Nuclear Hydrogen Initiative," Proceedings of ICAPP 2007, Paper 7530, Nice, France, May 13-18, 2007; *The Nuclear Renaissance at Work*, V. 5, Societe Francaise d'Energie Nucleaire – ICAPP 2007, pp. 2932-2940.
9. Yildiz, B., and Kazimi, M. S., "Efficiency of Hydrogen Production Systems Using Alternative Nuclear Energy Technologies," *Int. J. of Hydrogen Energy*, Vol. 31, pp. 77-92, 2006.
10. O'Brien, J. E., McKellar, M. G., and Herring, J. S., "Performance Predictions for Commercial-Scale High-Temperature Electrolysis Plants Coupled to Three Advanced Reactor Types," 2008 International Congress on Advances in Nuclear Power Plants, June 8-12, 2008, Anaheim, CA.
11. O'Brien, J. E., McKellar, M. G., Stoots, C. M., Herring, J. S., and Hawkes, G. L., "Parametric Study of Large-Scale Production of Syngas via High Temperature Electrolysis," in press, *International Journal of Hydrogen Energy*, 2009.
12. Stoots, C. M., O'Brien, J. E., "Results of Recent High-Temperature Co-electrolysis Studies at the Idaho National Laboratory," in press, *International Journal of Hydrogen Energy*, 2009.
13. Jensen, S. H., Larsen, P. H., Mogensen, M., "Hydrogen and synthetic fuel production from renewable energy sources," *Int. J. Hydrogen Energy*, Vol. 32, pp. 3253-3257, 2007
14. Mogensen, M., Jensen, S. H., Hauch, A., Chorkendorff, Ib., and Jacobsen, T., "Reversible Solid Oxide Cells*," Ceramic Engineering and Science Proceedings*, V 28, n 4, Advances in Solid Oxide Fuel Cells III - A Collection of Papers Presented at the 31st International Conference on Advanced Ceramics and Composites, 2008, p 91-101.
15. UniSim Design, R360 Build 12073, Copyright ©2005-2006 Honeywell International Inc.
16. O'Brien, J. E., Stoots, C. M., and Hawkes, G. L., "Comparison of a One-Dimensional Model of a High-Temperature Solid-Oxide Electrolysis Stack with CFD and Experimental Results," Proceedings, 2005 ASME International Mechanical Engineering Congress and Exposition, Orlando, Nov. 5 – 11, 2005.
17. O'Brien, J. E., "Thermodynamic Considerations for Thermal Water Splitting Processes and High-Temperature Electrolysis," 2008 ASME International Congress and Exposition, paper# IMECE2008-68880, Boston, Nov., 2008.
18. Brown, L. C., Lentsch, R. D., Besenbruch, G. E., Schultz, K. R., "Alternative Flowsheets for the Sulfur-Iodine Thermochemical Hydrogen Cycle," *AIChE Journal,* April 2003.
19. Forsberg, C. W., "Is Hydrogen the Future of Nuclear Energy?" Proceedings, International Topical Meeting on the Safety and Technology of Nuclear Hydrogen Production, Control, and Management, ANS Embedded Topical, 2007.
20. Harvego, E. A., McKellar, M. G., and O'Brien, J. E., "System Analysis of Nuclear-Assisted Syngas Production from Coal," *Journal of Engineering for Gas Turbines and Power*, Vol. 131, July, 2009.
21. McKellar, M. G., Hawkes, G. L., and O'Brien, J. E., "The Production of Syngas via High-Temperature Electrolysis and Bio-Mass Gasification, Proceedings of the 2008 ASME International Mechanical Engineering Congress and Exposition, paper# IMECE2008-68900, Boston, MA, Nov., 2008.
22. Harvego, E. A., McKellar, M. G., Sohal, M. S., O'Brien, J. E., and Herring, J. S., "Economic Analysis of a Nuclear Reactor Powered High Temperature Electrolysis Hydrogen Production Plant," ASME 2nd International Conference on Energy Sustainability, Jacksonville, FL, August 10-14, 2008.
23. Ivy, J., "Summary of Electrolytic Hydrogen Production," NREL Report NREL/MP-560-36734, September, 2004.